

Article

Numerical Wear Modeling in the Mixed and Boundary Lubrication Regime

Andreas Winkler * , Marcel Bartz  and Sandro Wartzack 

Engineering Design, Friedrich-Alexander-Universität Erlangen-Nürnberg, Martensstraße 9, 91058 Erlangen, Germany

* Correspondence: winkler@mfk.fau.de

Abstract: The increasing use of low-viscosity lubricants in order to reduce the friction in machine elements such as rolling bearings is leading to increased operation in the mixed or boundary lubrication regime. The associated wear can lead to an earlier failure of tribological systems. In this context, a detailed wear simulation offers great potential with regard to the design of machine elements as well as the calculation of lifetimes. This contribution presents an approach for the numerical wear simulation of lubricated rolling/sliding-contacts. Therefore, a finite element method-based simulation model was developed which is able to deal with non-Gaussian surfaces and contacts subject to boundary and mixed lubrication. Using the example of an axial cylindrical roller bearing considering realistic geometry, locally varying velocities, and two load cases, the wear modeling results of the mixed and the boundary lubrication regime were illustrated. The wear coefficient required for Archard's wear model was determined experimentally by means of a two-disc tribometer.

Keywords: wear modeling; contact mechanics; elastohydrodynamic lubrication; mixed lubrication; boundary lubrication; machine elements; thrust roller bearing; two-disc tribometer



Citation: Winkler, A.; Bartz, M.; Wartzack, S. Numerical Wear Modeling in the Mixed and Boundary Lubrication Regime. *Lubricants* **2022**, *10*, 334. <https://doi.org/10.3390/lubricants10120334>

Received: 14 November 2022

Accepted: 25 November 2022

Published: 26 November 2022

Publisher's Note: MDPI stays neutral with regard to jurisdictional claims in published maps and institutional affiliations.



Copyright: © 2022 by the authors. Licensee MDPI, Basel, Switzerland. This article is an open access article distributed under the terms and conditions of the Creative Commons Attribution (CC BY) license (<https://creativecommons.org/licenses/by/4.0/>).

1. Introduction

Holmberg and Erdemir [1] revealed that 20% of the world's energy consumption is attributed to overcoming friction. The use of low-viscosity lubricants is one way of reducing friction in tribological contacts. One disadvantage of this approach is that the increasing use of low-viscosity lubricants also leads to lower lubricant film thicknesses and thus to increased operation in the mixed or boundary lubrication regime. This in turn leads to an increase in wear in tribologically highly exposed machine elements. Since wear may result in catastrophic failures and operational breakdowns that can adversely impact productivity and cost, the prediction of wear in a reliable manner offers new possibilities for the understanding and redesigning of tribological systems. Therefore, numerical wear prediction has been the subject of numerous publications whose underlying simulation models analyze wear in dry and lubricated contacts.

Within this contribution, the finite element method-based simulation model of Winkler [2] was extended to include non-Gaussian surfaces and contacts subject to boundary lubrication in addition to contacts subject to mixed lubrication.

1.1. State-of-the-Art

Pödra et al. [3] developed a simulation model to calculate wear in a dry cylinder on flat and a ball on flat contact on the basis of the wear model according to Archard [4]. The calculation of the contact pressure was based on Winkler's foundation model [5]. Furthermore, Pödra et al. [6] published an FEM-based simulation model for wear calculation using the example of a pin on disc tribometer as well as a conical spinning contact.

Hegadekatte et al. [7–9] published a FEM-based wear simulation for both the dry pin on disc contact and the dry disc on disc contact. To consider the wear depth in the contact

calculation, Hegadekatte used the UMESHMOTION subroutine implemented in the FEM software ABAQUS.

Sfantos et al. [10] proposed a simulation method using the boundary element method (BEM) for dry sliding wear based on Archard's wear model, which was applied to both a pin on disc contact and a hip arthroplasty wear problem.

Andersson et al. [11] investigated the wear of a dry sphere on a flat contact. The contact pressure was calculated by a discrete convolution and fast Fourier transformation (DC-FFT) method utilizing the half-space theory and assuming linear elastic—perfectly plastic material behavior as described by Liu et al. [12].

Morales-Espejel et al. [13] recently published a simulation model for the example of an axial cylindrical roller bearing, which enables the local wear depth to be calculated on the basis of a FFT-based dry contact simulation and, in addition, the fatigue life can be calculated by damage accumulation according to Palmgren and Miner [14,15].

The approaches mentioned so far allow for the wear modeling of non-lubricated contacts. In the following, selected models for the numerical wear simulation of lubricated tribological systems are briefly described.

Zhu et al. [16] suggested an approach for the numerical wear calculation in lubricated contacts based upon a deterministic mixed elasto-hydrodynamic lubrication (EHL) model [17,18]. Thereby, the surface topography was directly incorporated into the film thickness equation and the wear volume was determined by means of Archard's wear model.

Lorentz et al. [19] developed a deterministic mixed lubrication micro-scale model considering two rough rubbing bodies, an adhesion model, heat generation as well as a lubrication domain. Reichert et al. [20] extended the model by wear calculation, whereas the wear coefficient for an Archard type wear model was determined based upon the Johnson–Cook damage law [21].

Terwey et al. [22–24] implemented a contact and wear model based upon half-space theory for boundary and mixed lubricated rolling contacts with a deterministic consideration of surface roughness. The contact pressure was determined by coupling an elastic half-space model with empirical lubricant film thickness equations according to [25]. The wear coefficient for Archard's wear model was determined by means of continuum damage mechanics (CDM) theory. In addition to the Archard wear equation, the wear model of Fleischer [26,27] was applied.

Beheshti et al. [28] introduced a stochastic approach for wear modeling in mixed lubricated line contacts based upon a load-sharing concept according to [29] and a CDM-based Archard type wear model considering simplified thermo-elasto-hydrodynamic analysis [30]. The asperity contact pressure was determined by means of the asperity contact model of Kogut and Etsion [31–33].

Zhang et al. [34] also investigated the wear as well as the surface roughness evolution in a mixed lubricated line contact. Therefore, the asperity contact model of Kogut and Etsion was coupled with a finite difference based EHL model to calculate the asperity and hydrodynamic contact pressures. Moreover, the change in surface height probability density function (PDF) was calculated in accordance with Sugimura and Kimura [35–37]. The modified PDF was subsequently used as an input for the stochastic asperity contact model in the next time step. Local wear was computed by Archard's wear law using the asperity contact pressure.

The aforementioned models represent only a small number of available numerical wear simulations. Further numerical wear simulation models can be found in the review paper of Mukras [38].

1.2. Derivation of the Need for Research

In summary, on one hand, simulation models for calculating wear in dry contacts and on the other hand, simulation models for lubricated contacts, have been developed. However, there is a lack of holistic methods for calculating the wear time efficiently across all lubrication regimes. For this reason, this paper presents an approach to numerical

wear modeling that covers the entire range from the mixed lubrication regime to boundary lubricated and dry contacts within a single simulation environment. The wear simulation is based on an EHL model for mixed lubricated contacts and a FEM based contact model for boundary lubricated and dry contacts, and it enables a time efficient wear calculation of lubricated and non-lubricated contraformal rolling/sliding contacts.

Due to its rather high sliding ratios and the associated susceptibility to wear, an axial cylindrical roller bearing operated in the mixed and boundary lubrication regime was selected as an example for the numerical wear simulation. The wear coefficient required for the numerical wear simulation was determined by means of experimental tests on a two-disc tribometer. Section 2 provides an overview of the theoretical fundamentals and the setup of the numerical simulation models, whereas Section 3 focuses on the experimental determination of wear coefficients as input variables for the numerical wear simulation.

2. Numerical Modeling

The numerical wear modeling of the raceways and washers of an axial cylindrical roller bearing was performed considering the coordinate system and velocity distribution shown in Figure 1.

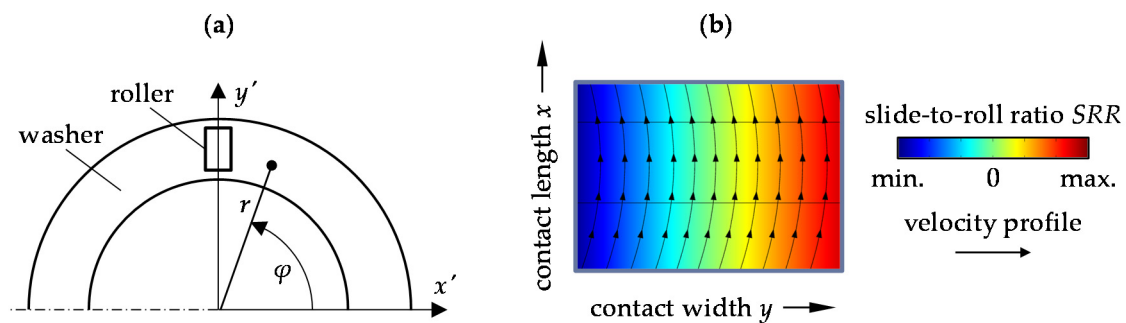


Figure 1. (a) Definition and location of coordinate systems; (b) schematic illustration of the velocity distribution in the contact area of the roller element and the raceway in a thrust roller bearing [2].

Unless otherwise indicated, the transition from the mixed to the boundary lubrication regime according to [39,40] can be assumed at a film thickness parameter

$$\lambda = \frac{h_{\min}}{\sqrt{\sigma_1^2 + \sigma_2^2}} \quad (1)$$

of $\lambda < 1$. However, it should be pointed out that the transition might also occur at significantly lower lubricant film thicknesses (see [41–43]).

The wear simulation model is part of the computation software TriboFEM, which is a FEM-based in-house tool of the Chair of Engineering Design at the Friedrich-Alexander-Universität Erlangen-Nürnberg for the simulation of elastohydrodynamically lubricated contacts. Within the framework of this contribution, the software was supplemented by the possibility of considering contacts subject to boundary lubrication as well as unlubricated contacts.

The following sections briefly describe the wear modeling approach in the area of mixed lubrication as well as in the area of boundary lubrication.

2.1. Mixed Lubrication Regime

Figure 2 shows the flowchart of the numerical wear modeling in the mixed lubrication regime. The implemented calculation models, which are detailed in the following sections, are highlighted in yellow. Instead of a transient simulation, a stationary EHL model was solved for each time step in order to save computing time. The wear depth was then extrapolated over a constant time step Δt .

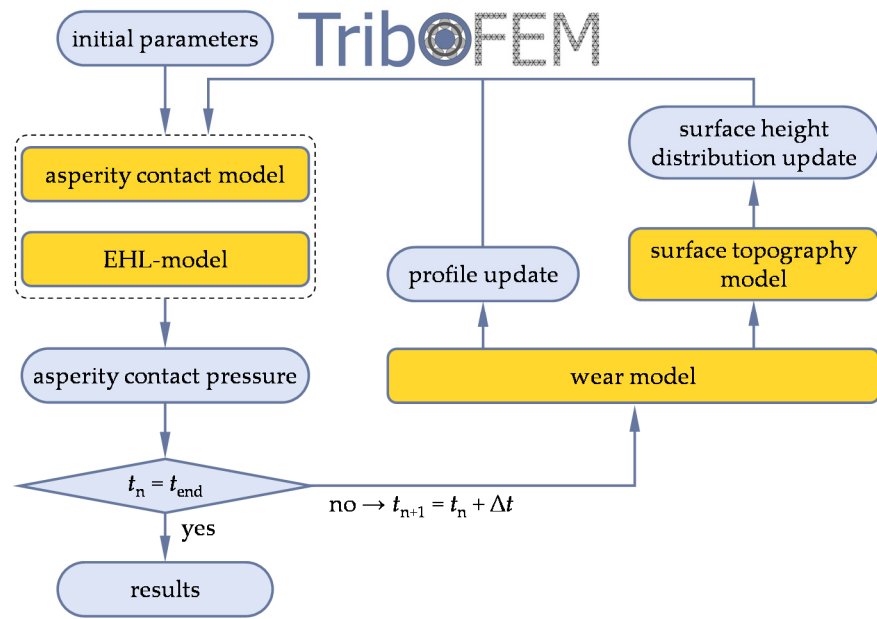


Figure 2. Flowchart of the solution scheme for the numerical wear calculation in the mixed lubrication regime.

2.1.1. Asperity Contact Model

The asperity contact model of Jackson and Green [44–46] was implemented within the present study. The underlying model for the contact of a rough surface with a rigid plane is shown in Figure 3. In order to stochastically describe the surface roughness, surface measurements were performed by means of laser scanning microscopy on three different rollers and washers of the axial cylindrical roller bearing type 81212.

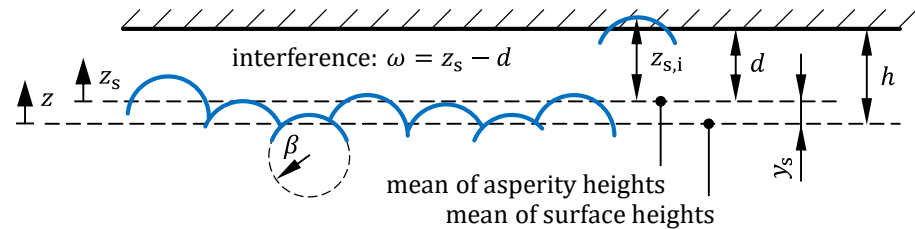


Figure 3. Contact of a rough surface with a smooth plane.

The relation between the separation of a rough surface and a rigid plane based on the asperity heights and surface heights can be written as

$$h = d + y_s \tag{2}$$

where y_s is the distance between the mean height of the asperity summits and the mean height of the surface according to Bush et al. [47]:

$$y_s = 4 \cdot \left(\frac{m_0}{\pi \cdot \alpha} \right)^{0,5} \tag{3}$$

Here, α denotes the bandwidth parameter

$$\alpha = \frac{m_0 \cdot m_4}{m_2^2} \tag{4}$$

which is calculated from the spectral moments of zeroth, second, and fourth order of a surface profile [48]:

$$\begin{aligned} m_0 &= E(z^2) = \sigma^2 \\ m_{2,x} &= E\left(\left(\frac{dz}{dx}\right)^2\right) & m_{2,y} &= E\left(\left(\frac{dz}{dy}\right)^2\right) & m_2 &= \sqrt{m_{2,x} \cdot m_{2,y}} \\ m_{4,x} &= E\left(\left(\frac{d^2z}{dx^2}\right)^2\right) & m_{4,y} &= E\left(\left(\frac{d^2z}{dy^2}\right)^2\right) & m_4 &= \sqrt{m_{4,x} \cdot m_{4,y}} \end{aligned} \quad (5)$$

Additionally, the spectral moments can be employed to determine the density of summits

$$\eta = \frac{m_4/m_2}{6 \cdot \pi \cdot \sqrt{3}} \quad (6)$$

as well as the mean summit radius

$$\beta = \frac{3}{8} \cdot \sqrt{\frac{\pi}{m_4}} \quad (7)$$

and the relation between the standard deviation of the surface heights σ and the standard deviation of the asperity heights σ_s

$$\sigma_s^2 = \left(1 - \frac{0.8968}{\alpha}\right) \cdot \sigma^2 \quad (8)$$

Aside from the parameters derived from the spectral moments, stochastic parameters of the surface profile such as standard deviation, skewness, and kurtosis are required in order to set up the PDF of surface heights:

$$\begin{aligned} S_q &= \sqrt{E\left((z - \mu)^2\right)} = \sigma \\ S_{sk} &= E\left(\left(\frac{z - \mu}{\sigma}\right)^3\right) \\ S_{ku} &= E\left(\left(\frac{z - \mu}{\sigma}\right)^4\right) \end{aligned} \quad (9)$$

It is worth mentioning that the origin of the z-axis was chosen so that $\mu = 0$.

The calculation of the integral asperity contact pressure for the contact of two rough surfaces requires equivalent values for the spectral moments [48]

$$\begin{aligned} m_{0,eq} &= m_{0,1} + m_{0,2} \\ m_{2,eq} &= m_{2,1} + m_{2,2} \\ m_{4,eq} &= m_{4,1} + m_{4,2} \end{aligned} \quad (10)$$

The standard deviation of the surface and asperity heights [49]

$$\sigma_{eq} = \sqrt{\sigma_1^2 + \sigma_2^2} \quad (11)$$

The mean summit radius

$$\frac{1}{\beta_{eq}} = \sqrt{\frac{1}{\beta_1^2} + \frac{1}{\beta_2^2}} \quad (12)$$

and the density of summits

$$\frac{1}{\eta_{eq}} = \frac{1}{\eta_1} \left(\frac{\beta_{eq}}{\beta_1}\right)^2 + \frac{1}{\eta_2} \left(\frac{\beta_{eq}}{\beta_2}\right)^2. \quad (13)$$

According to Tomota [50], the skewness and kurtosis of the equivalent rough surface is calculated according to Equations (14) and (15):

$$S_{sk,eq} = \frac{\sigma_1^3 \cdot S_{sk,1} + \sigma_2^3 \cdot S_{sk,2}}{\sigma_{eq}^3} \tag{14}$$

$$S_{ku,eq} = \frac{\sigma_1^4 \cdot S_{ku,1} + \sigma_2^4 \cdot S_{ku,2} + 6 \cdot \sigma_1^2 \cdot \sigma_2^2}{\sigma_{eq}^4} \tag{15}$$

The equivalent non-Gaussian PDF of the surface heights can be determined on the basis of Johnson’s system of frequency curves [51,52] using the equivalent standard deviation of the surface heights, the skewness, and kurtosis. The equivalent PDF of the asperity heights can be determined approximately from the PDF of the surface heights according to Yu [53]:

$$\phi_s(z_s) = \frac{1}{\sigma_s} \cdot \phi'_s\left(\frac{1}{\sigma_s} \cdot z_s\right) \approx \frac{1}{\sigma_s} \cdot \phi^*\left(\frac{1}{\sigma_s} \cdot z_s\right) = \frac{\sigma}{\sigma_s} \cdot \phi\left(\frac{\sigma}{\sigma_s} \cdot z_s\right) \tag{16}$$

Dimensionless values denoted by ‘ are normalized by the standard deviation of asperity heights σ_s , whereas dimensionless values denoted by * are normalized by the standard deviation of surface heights σ .

Finally, the asperity contact pressure according to the FEM-based elasto-plastic model of Jackson and Green [44–46] is given by:

$$p_a = \int_d^{d+1,9 \cdot \omega_c} \eta \cdot P_{el} \cdot \phi_s(z_s) dz_s + \int_{d+1,9 \cdot \omega_c}^{\infty} \eta \cdot P_{pl} \cdot \phi_s(z_s) dz_s \tag{17}$$

The elastic portion of the force acting on a single asperity is

$$P_{el} = \frac{4}{3} \cdot E' \cdot \beta^{0,5} \cdot \omega^{1,5} \tag{18}$$

with the equivalent Young’s modulus on both surfaces:

$$E' = \left(\frac{1 - \nu_1^2}{E_1} + \frac{1 - \nu_2^2}{E_2} \right)^{-1} \tag{19}$$

The plastic portion of the total asperity load is derived by a single asperity FEM simulation:

$$P_{pl} = \overline{P_c} \cdot \left\{ \left[\exp\left(-\frac{1}{4} \cdot \left(\frac{\omega}{\omega_c}\right)^{\frac{5}{12}}\right) \right] \cdot \left(\frac{\omega}{\omega_c}\right)^{\frac{3}{2}} + \frac{4 \cdot H_G}{C \cdot \sigma_y} \cdot \left[1 - \exp\left(-\frac{1}{25} \cdot \left(\frac{\omega}{\omega_c}\right)^{\frac{5}{9}}\right) \right] \cdot \frac{\omega}{\omega_c} \right\} \tag{20}$$

All parameters introduced in Equation (20) are calculated as follows:

$$\begin{aligned} \overline{P_c} &= \frac{4}{3} \cdot \left(\frac{\beta}{E'}\right)^2 \cdot \left(\frac{C}{2} \cdot \pi \cdot \sigma_y\right)^3 \\ B &= 0,14 \cdot \exp(23 \cdot e_y) \text{ with } e_y = \frac{\sigma_y}{E'} \\ C &= 1,295 \cdot \exp(0,736 \cdot \nu) \\ \frac{H_G}{\sigma_y} &= 2,84 \cdot \left[1 - \exp\left(-0,82 \cdot \left(\sqrt{\frac{\omega}{\beta}} \cdot \left(\frac{\omega}{1,9 \cdot \omega_c}\right)^{\frac{B}{2}}\right)^{-0,7}\right) \right] \end{aligned} \tag{21}$$

The Poisson’s ratio ν to be used in the above equation is that of the material that yields first. The critical interference is derived based upon the von Mises yield criterion:

$$\omega_c = \left(\frac{\pi \cdot C \cdot \sigma_y}{2 \cdot E'}\right)^2 \cdot \beta \tag{22}$$

2.1.2. EHL Model

The EHL simulation was carried out according to a FEM-based approach of Habchi [54] using commercial FEM software. Therefore, the Reynolds equation

$$\underbrace{\frac{\partial}{\partial x} \left(\frac{\rho(p_h) \cdot h(x,y)^3}{12 \cdot \eta(p_h)} \cdot \frac{\partial p_h}{\partial x} \right) + \frac{\partial}{\partial y} \left(\frac{\rho(p_h) \cdot h(x,y)^3}{12 \cdot \eta(p_h)} \cdot \frac{\partial p_h}{\partial y} \right)}_{\text{Poiseuille term}} = \underbrace{\frac{\partial}{\partial x} \left(\rho(p_h) \cdot h(x,y) \cdot \frac{u_1 + u_2}{2} \right) + \frac{\partial}{\partial y} \left(\rho(p_h) \cdot h(x,y) \cdot \frac{v_1 + v_2}{2} \right)}_{\text{Couette term}} \tag{23}$$

is solved in its weak form on the upper surface Ω_c of Figure 4 under consideration of a mass-conserving cavitation algorithm, as introduced by Marian et al. [55]. The Galerkin least squares (GLS) method [56] and isotropic diffusion (ID) method [57] were utilized for the numerical stabilization.

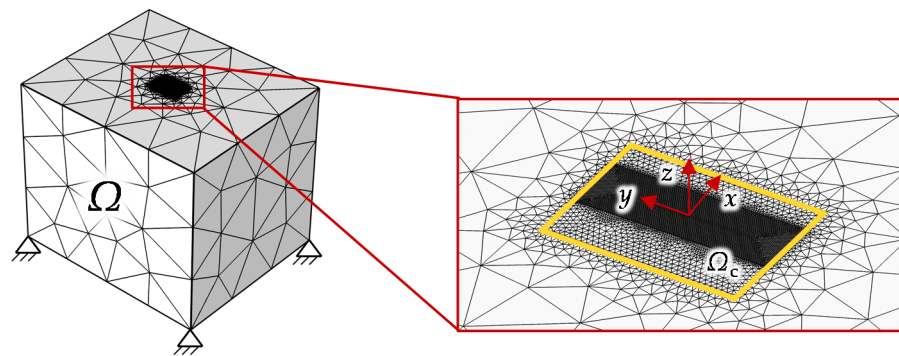


Figure 4. Geometry and meshing for the 3D FEM-based EHL-simulation of the mixed lubricated contact between the roller element and the raceway.

Density ρ and viscosity η were considered to be pressure-dependent following equations from Dowson and Higginson [58] and Roelands [59], respectively. The shear rate dependency of the viscosity was taken into account according to Eyring [60].

The elastic deformation is calculated for one equivalent body Ω with the Young’s modulus

$$E_{eq} = \frac{E_1^2 \cdot E_2 \cdot (1 + \nu_2)^2 + E_2^2 \cdot E_1 \cdot (1 + \nu_1)^2}{[E_1 \cdot (1 + \nu_2) + E_2 \cdot (1 + \nu_1)]^2} \tag{24}$$

and Poisson’s ratio

$$\nu_{eq} = \frac{E_1 \cdot \nu_2 \cdot (1 + \nu_2) + E_2 \cdot \nu_1 \cdot (1 + \nu_1)}{E_1 \cdot (1 + \nu_2) + E_2 \cdot (1 + \nu_1)} \tag{25}$$

The lubricant film thickness equation describes the height of the separating fluid film in terms of the distance h_0 and the shape of the undeformed geometry s_0 as well as of the elastic deformation δ and the wear depth h_{wear} :

$$h(x, y, t_n) = h_0(t_n) + s_0(x, y) + h_{wear}(x, y, t_n) + \delta(x, y, t_n) \tag{26}$$

Here, s_0 is a function describing the equivalent undeformed geometry considering logarithmically profiled rolling elements:

$$s_0(x, y) = \frac{x^2}{D} + 0.00035 \cdot D \cdot \ln \left(\frac{1}{1 - \left(\frac{2 \cdot y}{L} \right)^2} \right) \tag{27}$$

The load balance equation ensures the equilibrium of forces:

$$F = \iint_{\Omega_c} (p_h(x, y) + p_a(x, y)) dx dy \tag{28}$$

This considers both the hydrodynamic contact pressure as well as the asperity contact pressure in the mixed lubrication regime.

2.1.3. Wear Model

The local wear depth is determined by applying the wear model according to Archard [4]:

$$h_{wear}(x, y, t_n) = h_{wear}(x, y, t_{n-1}) + k \cdot p_a(x, y, t_n) \cdot v_{slide}(x, y) \cdot \Delta t \tag{29}$$

Since only the asperity contact pressure p_a is used for the wear calculation, the wear coefficient k can thus be determined independently of the lubricant film thickness in the boundary lubrication regime. Furthermore, v_{slide} denotes the local sliding velocity.

The wear coefficient depends on numerous factors such as the material properties, surface conditions, and boundary layers. It is frequently determined experimentally and can vary between 10^{-1} and 10^{-15} mm³/Nm for metals [61,62]. Within the framework of this study, the wear coefficient required for the wear simulation was determined experimentally on a two-disc tribometer (see Section 3).

2.1.4. Surface Topography Model

The surface topography of Sugimura and Kimura [35–37] allows for the calculation of the time-varying change of the probability density function of the surface heights as a function of the wear depth (see Figure 5).

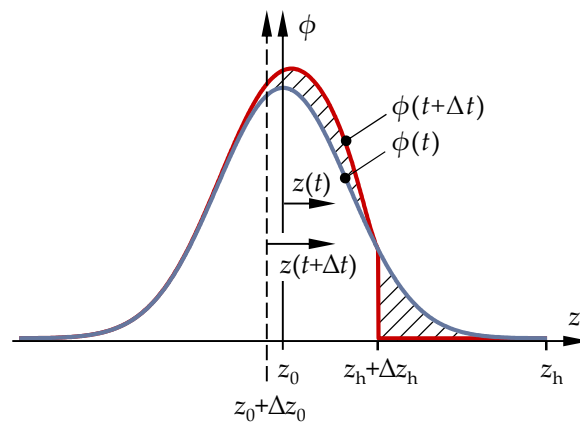


Figure 5. Evolution of the surface height distribution $\phi(z)$ during the time interval Δt .

The density function at time $t + \Delta t$ is calculated from Equation (30):

$$\phi(z, t + \Delta t) = \begin{cases} \phi(z + \Delta z_0, t) + \psi(z_h + \Delta z_h - z) \cdot \Delta \phi(t), & z \leq z_h + \Delta z_h \\ 0, & z > z_h + \Delta z_h \end{cases} \tag{30}$$

Thereby, ψ denotes the probability density function of the wear-induced height loss. Jeng [63–65] further extended the model of Sugimura and Kimura to include non-Gaussian PDFs using Johnson’s system of frequency curves [51,52]. For further information on the surface topography model of Sugimura and Kimura and its numerical implementation, see [2].

2.2. Boundary Lubrication Regime and Dry Contacts

Figure 6 shows the flowchart of the numerical wear modeling in the boundary lubrication regime.

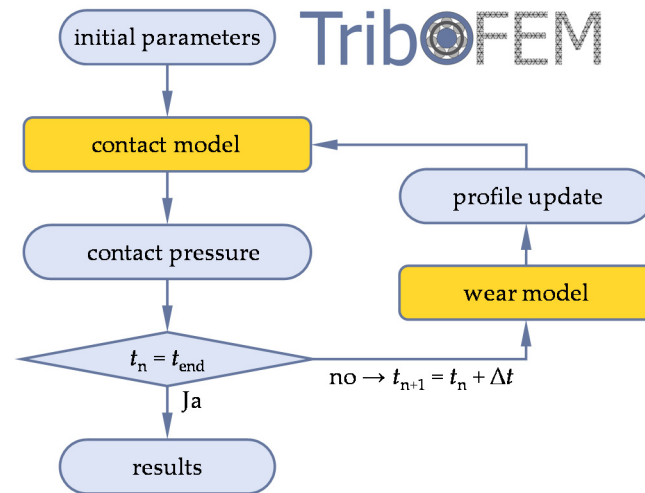


Figure 6. Flowchart of the solution scheme for the numerical wear calculation in the boundary lubrication regime.

Contrary to the load-sharing concept of the wear simulation in the mixed lubrication regime, it was assumed that there was no supporting hydrodynamic lubricant film present in the area of boundary lubrication. For this reason, the differences to Section 2.1 will be discussed in the following.

2.2.1. Contact Model

In distinction to the wear simulation of contacts subject to mixed lubrication, in the area of boundary lubrication and dry contacts, a FEM contact model based on the penalty contact algorithm with an equivalent body was used to calculate the contact pressure. Analogous to the EHL modeling approach according to Habchi [54], a cubic substitute body is defined, which possesses the equivalent mechanical properties of the base and the counter body. This body is brought into contact with a rigid surface, which in turn has the equivalent geometry of both bodies (see Figure 7).

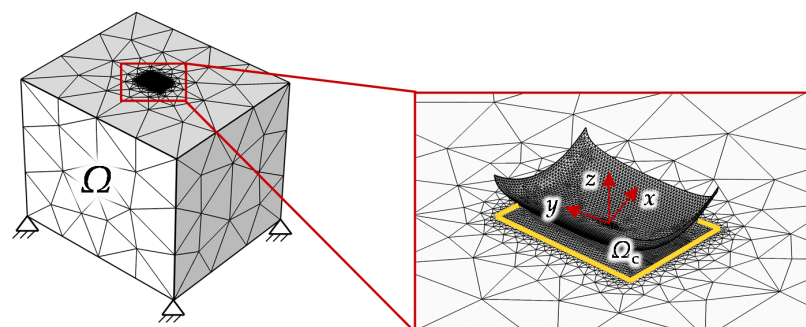


Figure 7. Geometry and meshing for the 3D FEM-based contact simulation of the boundary lubricated contact between the roller element and the raceway.

The consideration of the wear-related profile change in the contact simulation was achieved by an adaptation of the Karush–Kuhn–Tucker contact conditions, as depicted in Figure 8.

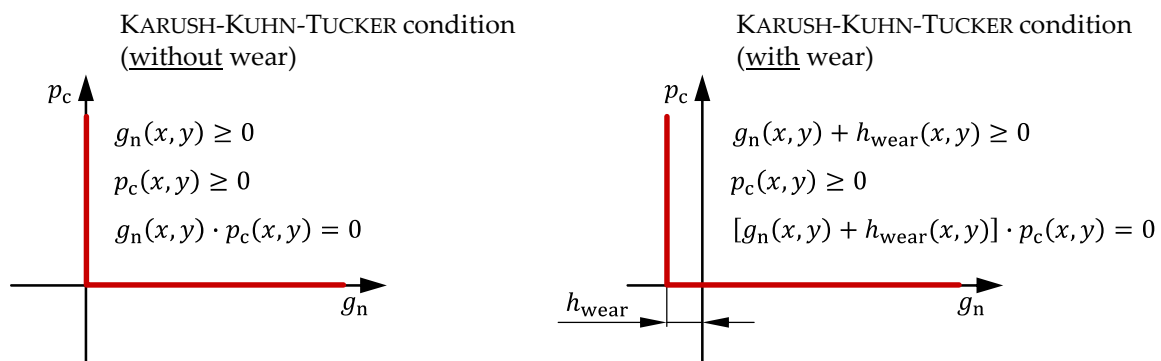


Figure 8. Wear-related modification of the Karush–Kuhn–Tucker condition.

The parameter g_n denotes the distance of the rigid surface to the elastic cubic body. The Karush–Kuhn–Tucker conditions can be modified within the wear simulation to allow for the penetration of both bodies in the amount of the local wear depth h_{wear} in order to consider the wear-related profile change in the contact pressure calculation. As an alternative to varying the Karush–Kuhn–Tucker conditions, the geometry function of the rigid surface can be extended by a wear term, analogous to Equation (26).

2.2.2. Wear Model

Archard's wear model was applied to the total contact pressure p_c determined by the contact model presented in the previous section:

$$h_{\text{wear}}(x, y, t_n) = h_{\text{wear}}(x, y, t_{n-1}) + k \cdot p_c(x, y, t_n) \cdot v_{\text{slide}}(x, y) \cdot \Delta t \quad (31)$$

In both the mixed lubricated and boundary lubricated systems, the wear coefficient was determined experimentally in the boundary lubrication regime. Further details regarding the experimental determination of wear coefficients by means of a two-disc tribometer can be found in Section 3.

3. Experimental Determination of Wear Coefficients

A two-disc tribometer—as depicted in Figure 9 was chosen as an experimental set-up to determine the wear coefficient as an input parameter for the numerical wear simulations. The tribometer consists of two independently driven spindles that rotate the test discs at a defined speed and press them against each other at a defined force. The contact between both discs is lubricated by circulating oil, which can be warmed up to a defined temperature by oil heating.

The test discs were made of the rolling bearing steel 100Cr6 and had the properties listed in Table 1. One washer was cylindrical, while the other washer was crowned with a radius of 50 mm. A non-additivated PAO 6 was used as the lubricant, which was heated to 80 °C.

Table 1. Test parameters for the two-disc tribometer.

Parameter	Value
Disc material	100Cr6
Lubricant	PAO 6
Oil temperature	80 °C
Disc 1	Ø 45 mm; Crowning: 50 mm
Disc 2	Ø 45 mm; Crowning: ∞

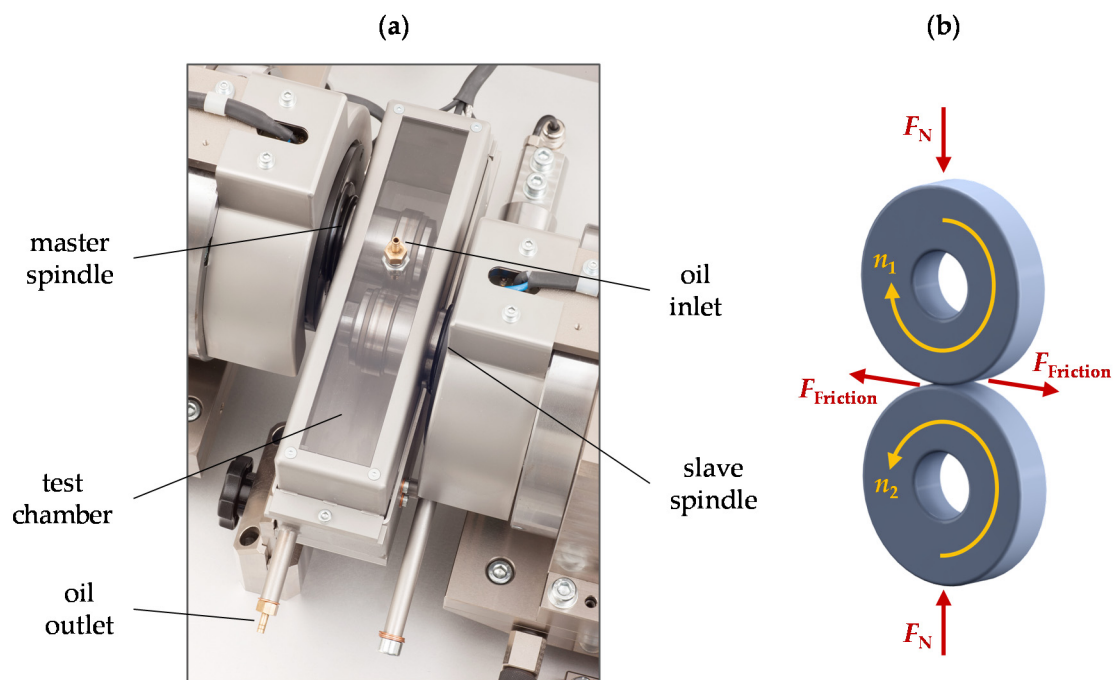


Figure 9. (a) View into the test chamber of the two-disc tribometer. (b) Schematic illustration of the contact of two test discs.

Three replicate trials were conducted, each lasting 72 h. The normal force was 500 N and the speeds of the master and slave spindles were set to 30 rpm and 10 rpm, respectively. This resulted in a maximum Hertzian pressure of approximately 1.4 GPa and a slide-to-roll ratio (SRR) of 100%. Furthermore, the lubricant film thickness parameter λ was about 0.18, whereby the minimum lubricant film thickness h_{\min} was estimated according to Hamrock's empirical equation for elliptical contacts [66]. The wear coefficient was determined in the boundary lubrication regime, as only the solid contact pressure was applied in Archard's wear model (see Equations (29) and (31)). The experimental validation of this approach is part of ongoing research.

The evaluation of the wear volume to calculate a wear coefficient was achieved by two methods. On one hand, the surface profile of the discs was measured at four positions evenly distributed around the circumference before and after the test by the Stylus instrument Form Talysurf[®] PGI NOVUS. By creating a difference profile, the wear cross-sectional area A_w could be determined:

$$A_w = \frac{1}{N} \cdot \sum_{i=1}^N A_{w,i} \quad (32)$$

Furthermore, the wear volume as well as the wear coefficient could be calculated from the wear cross-sectional area A_w , the diameter of the test discs D_{disc} , the normal force F , and the sliding distance s :

$$k = \frac{W}{F \cdot s} = \frac{A_w \cdot \pi \cdot D_{\text{disc}}}{F \cdot s} \quad (33)$$

Figures 10 and 11 show exemplary plots of a difference profile of a crowned and a cylindrical disc, respectively.

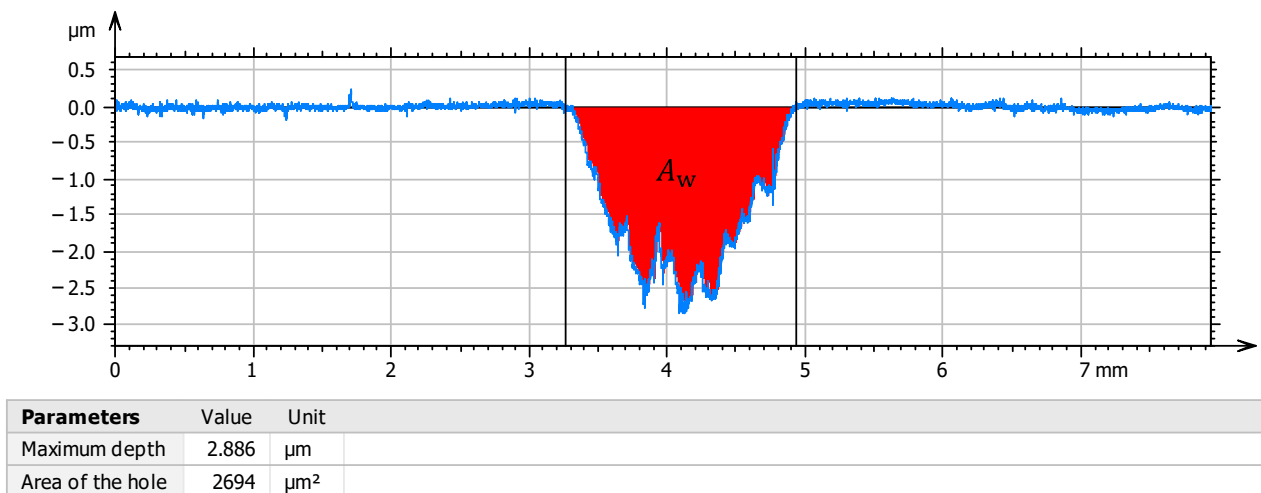


Figure 10. Exemplary profile difference of a crowned disc.

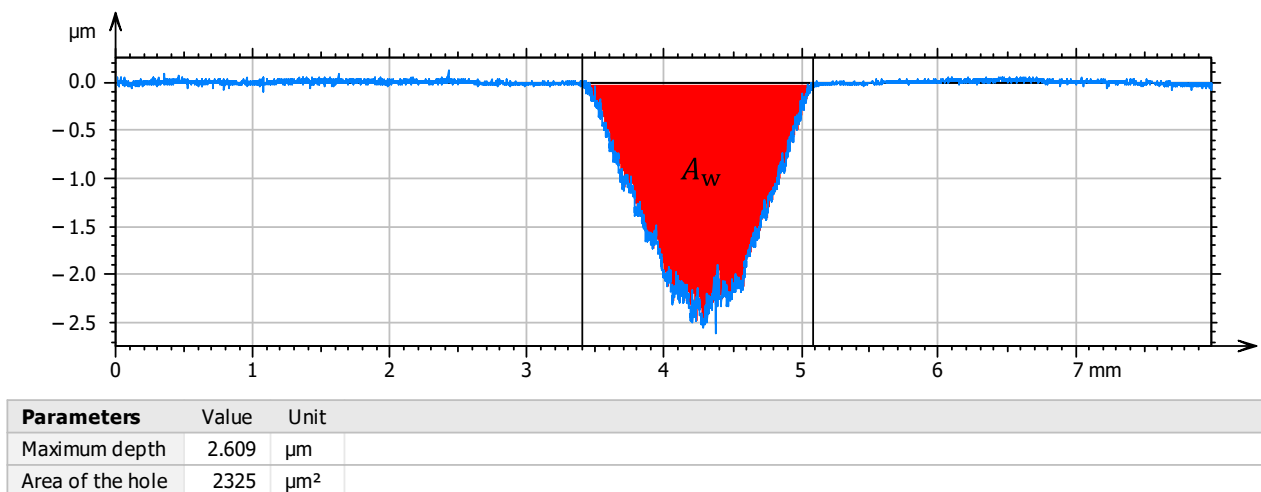


Figure 11. Exemplary profile difference of a cylindrical disc.

On the other hand, the wear volume was determined gravimetrically by weighing the discs before and after the test using a Kern[®] ALJ 500-4A analytical balance.

$$m_{\text{start}} = \frac{1}{N} \cdot \sum_{i=1}^N m_{\text{start},i} \quad (34)$$

$$m_{\text{end}} = \frac{1}{N} \cdot \sum_{i=1}^N m_{\text{end},i} \quad (35)$$

In this way, the wear coefficient can similarly be calculated from the difference of masses and the density of the disc material ρ :

$$k = \frac{W}{F \cdot s} = \frac{m_{\text{start}} - m_{\text{end}}}{\rho \cdot F \cdot s} \quad (36)$$

Both approaches were in very good accordance with each other. While the method using a stylus instrument revealed an average wear coefficient of $k = 1,21 \cdot 10^{-7} \frac{\text{mm}^3}{\text{Nm}}$, the gravimetric method resulted in an average wear coefficient of $k = 1,22 \cdot 10^{-7} \frac{\text{mm}^3}{\text{Nm}}$.

4. Results and Discussion

In this section, exemplary simulation results for two different operating conditions of the axial cylindrical roller bearing 81212 are discussed. An overview of the investigated load cases can be found in Table 2.

Table 2. Load cases for the numerical wear simulation.

Operating Parameters	Load Case 1 (Mixed Lubrication)	Load Case 2 (Boundary Lubrication)
Operating time t	8 h	80 h
Rotational speed n	1000 min^{-1}	100 min^{-1}
Load F	50 kN	
Lubricant	PAO 6 at 80 °C	

The contact geometry was based on the dimensions of the axial cylindrical roller bearing 81212. The experimentally determined wear coefficient as presented in Section 3 for Archard's wear model was applied within the wear simulation. Moreover, the non-Gaussian PDF of the surface and asperity heights required for the stochastic asperity contact model of Jackson and Green as well as the surface topography model of Sugimura and Kimura were determined by measurements on bearing washers and rolling elements of the axial cylindrical roller bearing 81212 using the 3D laser scanning microscope Keyence® VK-X200 (Keyence Corporation, Osaka, Japan). For the rolling bearing steel 100Cr6, a Young's modulus of 208 GPa and a Poisson's ratio of 0.3 were assumed. The oil was assumed to be structurally viscous with a shear rate dependency according to Eyring with an Eyring stress of $\tau_E = 10$ MPa.

The selected operating parameters resulted in 3,600,000 overrollings for both load cases. In the mixed lubrication regime of load case 1, the lubricant film thickness parameter was $\lambda \approx 0.64$; in the boundary lubrication regime of load case 2, it amounted to $\lambda \approx 0.13$. According to deterministic numerical investigations by Terwey [22], the transition between the mixed and boundary lubrication for the specific axial cylindrical roller bearing under consideration occurred at a lubricant film thickness parameter of $\lambda \approx 0.35$.

Figure 12 illustrates the initial hydrodynamic and asperity contact pressure for load case 1 and the total contact pressure for load case 2, respectively. The pressure was evaluated at the contact center ($y = 0$) in the rolling direction (i.e., along the x -coordinate).

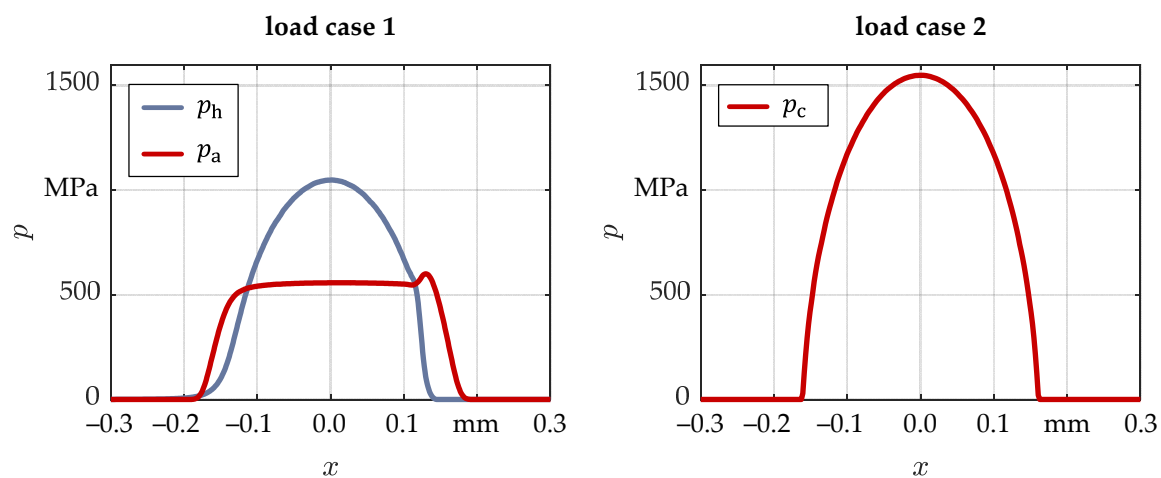


Figure 12. Initial contact pressure along the x -coordinate for load cases 1 and 2.

Figure 13 shows the distribution of the total contact pressures over the whole contact area at the initial state and after 3,600,000 overrollings. The initial contact pressure of the contact subject to mixed lubrication (load case 1) differed slightly from the contact pressure

of the boundary lubricated contact (load case 2), as heavily loaded, mixed lubricated EHL contacts typically show a steeper pressure gradient at the contact outlet compared to the Hertz-like contact pressure of load case 2 in the boundary lubrication regime. After 3,600,000 overrollings, a significant pressure peak in the center of the contact occurred, which was more pronounced in load case 2 than in load case 1.

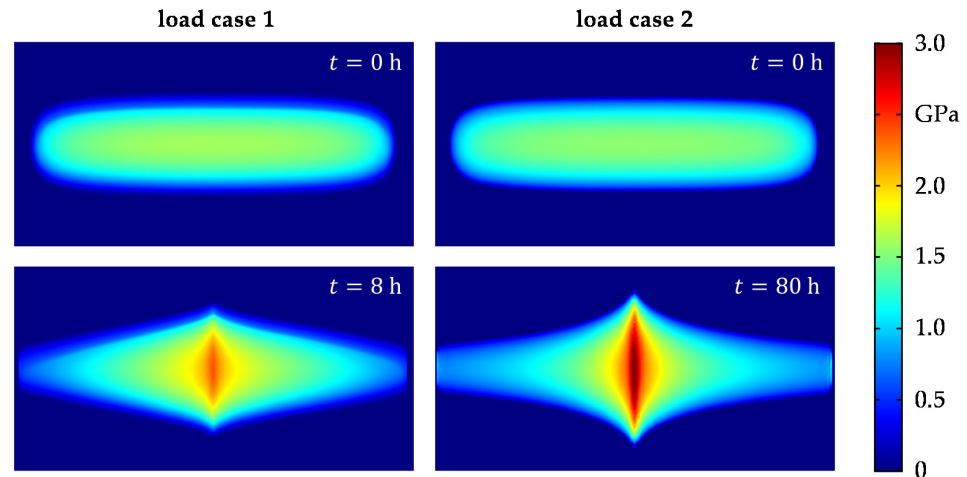


Figure 13. Total contact pressure at the initial state and after 3,600,000 overrollings.

The reason for the pressure peaks resulted from the wear depth profiles shown in Figure 14. The wear depths were calculated according to Equations (29) and (31), by a superposition of contact pressure and sliding speed. While pure rolling occurs in the center of the rolling element, the sliding velocity increases linearly toward the outer and inner direction (see Figure 1b). The slightly higher wear depths on the inner contact halves (negative y -direction) of the bearing washers can be explained by the distribution of the wear volume over a smaller circumference compared to the outer sides. It should be noted that in experimental tests, wear can also occur in the contact center due to macroscopic slip and displacement of the rollers in the radial direction, which would result in lower contact pressures.

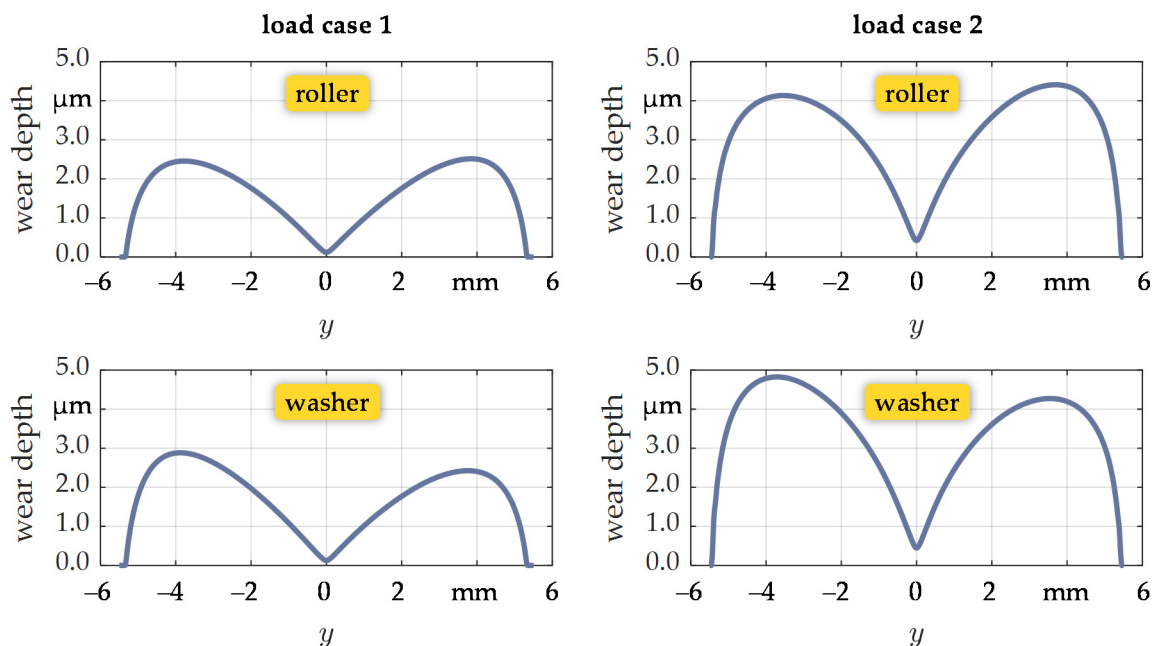


Figure 14. Wear depths after 3,600,000 overrollings.

Finally, the results of the stochastic asperity contact model according to Greenwood and Williamson and the surface topography model according to Sugimura and Kimura are illustrated Figure 15. Figure 15a shows the probability density function of the equivalent rough surface of the washer and roller at the initial state (blue) and after 3,600,000 overrollings (red). The suitability of the Sugimura and Kimura model for the prediction of the PDF of worn surfaces has already been experimentally investigated and confirmed by [37] and [64,65]. Using the PDF of asperity heights ϕ_s , the asperity contact pressure curves shown in Figure 15b were obtained. It is apparent that the transition from a state of full film lubrication to the regime of mixed lubrication shifted toward lower lubricant film thicknesses due to the wear-related modification of the surface roughness. Furthermore, Figure 15c shows the evolution of the equivalent standard deviation of surface heights σ_{eq} . After approximately 3 h, a stationary state of the surface roughness was reached.

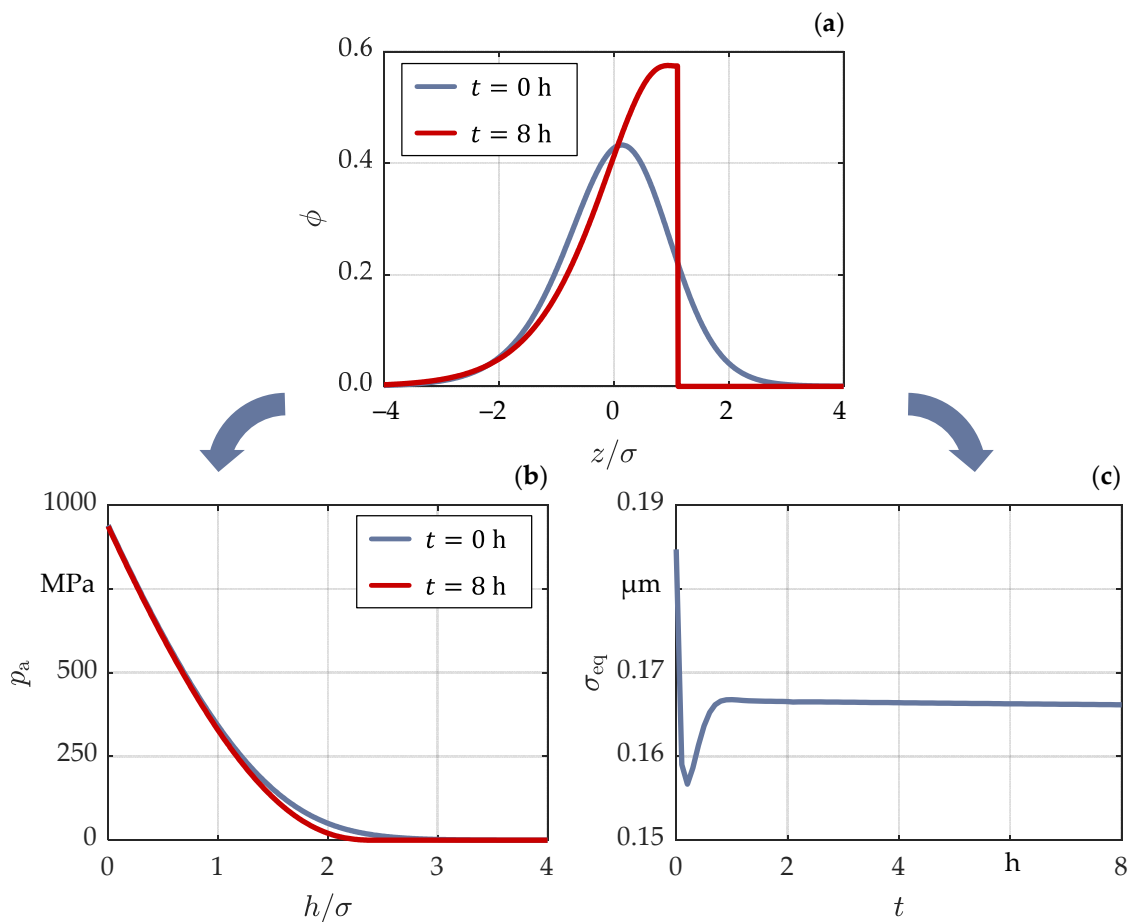


Figure 15. Results of the wear simulation in the mixed lubrication regime: (a) PDF of the surface heights at the initial state and after 3,600,000 overrollings; (b) asperity contact pressure curve at the initial state and after 3,600,000 overrollings; (c) equivalent standard deviation of surface heights over time.

The total wear masses of both bearing washers and all 15 rolling elements are summarized in Table 3.

Table 3. Calculated wear masses after 3,600,000 overrollings.

	Load Case 1 (Mixed Lubrication)	Load Case 2 (Boundary Lubrication)
Wear mass	144 mg	280 mg

In order to evaluate the presented simulation results with respect to their accuracy, experimental investigations are part of the currently ongoing research. The roller bearing test apparatus FE8 [67,68] was identified as a suitable test rig for the experimental validation.

5. Conclusions and Outlook

A detailed wear simulation can contribute to estimating the service life of machine elements and to avoiding premature failure of machine elements as well as avoiding operating conditions that are most subjected to wear. It can additionally support the optimization of contact geometries. The wear modeling approach presented within this contribution provides a detailed wear calculation of rolling/sliding contacts, which are operated in the mixed and boundary lubrication regime as well as under unlubricated conditions. The contact calculation in the mixed lubrication regime is based on an EHL simulation, which is coupled with a stochastic asperity contact model via the load-sharing concept. In the region of boundary lubrication and dry friction, the contact pressure is determined via a FEM-based “half-space”-like contact model. In addition to axial cylindrical roller bearings, the presented wear simulation approach can be applied to other types of rolling bearings and further machine elements such as gears or cam-tappets.

In order to obtain reliable quantitative predictions of wear, an adequate experimental determination of the wear coefficient k for the respective tribological system is of utmost importance. In this contribution, the experimental determination of a wear coefficient using a two-disc tribometer was described. Furthermore, to verify the accuracy of the wear simulation, a comparison with experimental tests on a component test rig is required. The latter is currently part of ongoing investigations by means of the roller bearing test apparatus FE8.

Author Contributions: Conceptualization, A.W.; Methodology, A.W.; Software, A.W.; Experimental investigations, A.W.; Formal analysis, A.W.; Writing—original draft preparation, A.W.; Writing—review and editing, A.W., M.B. and S.W.; Visualization, A.W.; Supervision, M.B. and S.W. All authors have read and agreed to the published version of the manuscript.

Funding: This research received no external funding.

Data Availability Statement: Not applicable.

Acknowledgments: We acknowledge the financial support by Friedrich-Alexander-Universität Erlangen-Nürnberg within the funding programme “Open Access Publication Funding”.

Conflicts of Interest: The authors declare no conflict of interest.

Nomenclature

A_w	Wear cross-sectional area
B	Parameter of the Jackson/Green asperity contact model
C	Parameter of the Jackson/Green asperity contact model
d	Separation based on asperity heights
D	Diameter of roller
D_{disc}	Diameter of test discs
E	Young’s modulus
E'	Combined Young’s modulus of two surfaces for the asperity contact model
E_{eq}	Equivalent Young’s modulus
F	Load
g_n	Distance between master and slave surfaces of FEM-based contact models
h	Separation based on surface heights / lubricant film thickness
h_0	Film thickness constant parameter
h_{min}	Minimum lubricant film thickness
h_{wear}	Local wear depth
H_G	Geometrical hardness limit according to the Jackson/Green asperity contact model

k	Wear coefficient
L	Length of roller
$m_{0,2,4}$	Zeroth, second, and fourth spectral moment of a surface profile
$m_{\text{start}}, m_{\text{end}}$	Masses of discs before and after two-disc tribometer tests
n	Rotational speed
p_a	Asperity contact pressure
p_c	Total contact pressure in boundary lubricated or dry contacts
p_h	Hydrodynamic contact pressure
\bar{P}_c	Critical contact force at initial yielding according to the Jackson/Green asperity contact model
P_{el}	Elastic portion of the force acting on a single asperity
P_{pl}	Plastic portion of the force acting on a single asperity
s	Sliding distance
s_0	Geometry-function of the roller
S_q	Standard deviation of surface heights
S_{sk}	Skewness of surface heights
S_{ku}	Kurtosis of surface heights
SRR	Slide-to-roll ratio
t	Time
u_1, u_2	Relative velocity of the washer/roller in x direction
v_1, v_2	Relative velocity of the washer/roller in y direction
v_{slide}	Sliding velocity
x, y	Coordinates in and perpendicular to the rolling direction
y_s	Distance between the mean height of asperities and the mean height of surface
z	Profile coordinate based on mean height of surface
z_s	Profile coordinate based on mean height of asperities
z_0	Ordinate of the mean line of the composite profile
Δz_0	Descending quantity of mean line
z_h	Highest point of composite profile
Δz_h	Moving distance of highest point
α	Bandwidth parameter
β	Mean summit radius
δ	Elastic deformation in z direction
λ	Dimensionless film thickness parameter
ν_1, ν_2	Poisson's ratio of washer/roller
ν_{eq}	Equivalent Poisson's ratio
ρ	Density
η	Area density of asperities
η	Dynamic viscosity
σ	Standard deviation of surface heights
σ_s	Standard deviation of asperity heights
σ_y	Yield strength
ϕ	Probability density function of surface heights
ϕ_s	Probability density function of asperity heights
ψ	Height-loss probability density function
ω	Interference
ω_c	Critical interference

References

- Holmberg, K.; Erdemir, A. Influence of tribology on global energy consumption, costs and emissions. *Friction* **2017**, *5*, 263–284. [[CrossRef](#)]
- Winkler, A.; Marian, M.; Tremmel, S.; Wartzack, S. Numerical Modeling of Wear in a Thrust Roller Bearing under Mixed Elastohydrodynamic Lubrication. *Lubricants* **2020**, *8*, 58. [[CrossRef](#)]
- Pödra, P.; Andersson, S. Wear simulation with the Winkler surface model. *Wear* **1997**, *207*, 79–85. [[CrossRef](#)]
- Archard, J.F.; Hirst, W. The wear of metals under unlubricated conditions. *Proc. R. Soc. Lond. Ser. A. Math. Phys. Eng. Sci.* **1956**, *236*, 397–410. [[CrossRef](#)]
- Winkler, E. *Die Lehre von der Elastizität und Festigkeit mit besonderer Rücksicht auf ihre Anwendung in der Technik: Für polytechnische Schulen, Bauakademien, Ingenieure, Maschinenbauer, Architekten, etc.*; Dominicus: Prag, Czech Republic, 1867.

6. Pödra, P.; Andersson, S. Simulating sliding wear with finite element method. *Tribol. Int.* **1999**, *32*, 71–81. [[CrossRef](#)]
7. Hegadekatte, V.; Huber, N.; Kraft, O. Finite element based simulation of dry sliding wear. *Model. Simul. Mater. Sci. Eng.* **2005**, *13*, 57–75. [[CrossRef](#)]
8. Hegadekatte, V.; Huber, N.; Kraft, O. Modeling and simulation of wear in a pin on disc tribometer. *Tribol. Lett.* **2006**, *24*, 51–60. [[CrossRef](#)]
9. Hegadekatte, V.; Kurzenhäuser, S.; Huber, N.; Kraft, O. A predictive modeling scheme for wear in tribometers. *Tribol. Int.* **2008**, *41*, 1020–1031. [[CrossRef](#)]
10. Sfantos, G.K.; Aliabadi, M.H. A boundary element formulation for three-dimensional sliding wear simulation. *Wear* **2007**, *262*, 672–683. [[CrossRef](#)]
11. Andersson, J.; Almqvist, A.; Larsson, R. Numerical simulation of a wear experiment. *Wear* **2011**, *271*, 2947–2952. [[CrossRef](#)]
12. Liu, S.; Wang, Q.; Liu, G. A versatile method of discrete convolution and FFT (DC-FFT) for contact analyses. *Wear* **2000**, *243*, 101–111. [[CrossRef](#)]
13. Morales-Espejel, G.E.; Gabelli, A. Rolling bearing seizure and sliding effects on fatigue life. *Proc. Inst. Mech. Eng. Part J J. Eng. Tribol.* **2019**, *233*, 339–354. [[CrossRef](#)]
14. Palmgren, A. Die Lebensdauer von Kugellagern: Durability of Ball Bearings. *Z. Des Ver. Dtsch. Ing.* **1924**, *68*, 339–341.
15. Miner, M.A. Cumulative Damage in Fatigue. *J. Appl. Mech.* **1945**, *12*, 159–164. [[CrossRef](#)]
16. Zhu, D.; Martini, A.; Wang, W.; Hu, Y.; Lisowsky, B.; Wang, Q.J. Simulation of Sliding Wear in Mixed Lubrication. *J. Tribol.* **2007**, *129*, 544–552. [[CrossRef](#)]
17. Zhu, D.; Hu, Y.-Z. A Computer Program Package for the Prediction of EHL and Mixed Lubrication Characteristics, Friction, Subsurface Stresses and Flash Temperatures Based on Measured 3-D Surface Roughness. *Tribol. Trans.* **2001**, *44*, 383–390. [[CrossRef](#)]
18. Hu, Y.-Z.; Zhu, D. A Full Numerical Solution to the Mixed Lubrication in Point Contacts. *J. Tribol.* **2000**, *122*, 1–9. [[CrossRef](#)]
19. Lorentz, B.; Albers, A. A numerical model for mixed lubrication taking into account surface topography, tangential adhesion effects and plastic deformations. *Tribol. Int.* **2013**, *59*, 259–266. [[CrossRef](#)]
20. Reichert, S.; Lorentz, B.; Heldmaier, S.; Albers, A. Wear simulation in non-lubricated and mixed lubricated contacts taking into account the microscale roughness. *Tribol. Int.* **2016**, *100*, 272–279. [[CrossRef](#)]
21. Johnson, G.R.; Cook, W.H. Fracture characteristics of three metals subjected to various strains, strain rates, temperatures and pressures. *Eng. Fract. Mech.* **1985**, *21*, 31–48. [[CrossRef](#)]
22. Terwey, J.T. Näherungslösungen für Reibung und Verschleiß in ölgeschmierten Wälzkontakten unter Berücksichtigung der realen Rheologie. Ph.D. Thesis, Gottfried Wilhelm Leibniz Universität Hannover, Hannover, Germany, 2020.
23. Terwey, J.T.; Berninger, S.; Burghardt, G.; Jacobs, G.; Poll, G. Numerical Calculation of Local Adhesive Wear in Machine Elements Under Boundary Lubrication Considering the Surface Roughness. In *Proceedings of the 7th International Conference on Fracture Fatigue and Wear*; Abdel Wahab, M., Ed.; Springer: Singapore, 2019; pp. 796–807, ISBN 9789811344091.
24. Terwey, J.T.; Fourati, M.A.; Pape, F.; Poll, G. Energy-Based Modelling of Adhesive Wear in the Mixed Lubrication Regime. *Lubricants* **2020**, *8*, 16. [[CrossRef](#)]
25. Hamrock, B.J.; Schmid, S.R.; Jacobson, B.O. *Fundamentals of Fluid Film Lubrication*, 2nd ed.; Marcel Dekker: New York, NY, USA, 2004; ISBN 9780824753719.
26. Fleischer, G. *Verschleiß und Zuverlässigkeit*; VEB: Berlin, Germany, 1980.
27. Fleischer, G. Zur Energetik der Reibung. *Wiss. Z. Der Tech. Univ. Otto Von Guericke Magdebg.* **1990**, *34*, 55–66.
28. Beheshti, A.; Khonsari, M.M. An engineering approach for the prediction of wear in mixed lubricated contacts. *Wear* **2013**, *308*, 121–131. [[CrossRef](#)]
29. Johnson, K.L.; Greenwood, J.A.; Poon, S.Y. A simple theory of asperity contact in elastohydro-dynamic lubrication. *Wear* **1972**, *19*, 91–108. [[CrossRef](#)]
30. Beheshti, A.; Khonsari, M.M. A Thermodynamic Approach for Prediction of Wear Coefficient Under Unlubricated Sliding Condition. *Tribol. Lett.* **2010**, *38*, 347–354. [[CrossRef](#)]
31. Kogut, L.; Etsion, I. Elastic-Plastic Contact Analysis of a Sphere and a Rigid Flat. *J. Appl. Mech.* **2002**, *69*, 657–662. [[CrossRef](#)]
32. Kogut, L.; Etsion, I. A Finite Element Based Elastic-Plastic Model for the Contact of Rough Surfaces. *Tribol. Trans.* **2003**, *46*, 383–390. [[CrossRef](#)]
33. Kogut, L.; Etsion, I. A Static Friction Model for Elastic-Plastic Contacting Rough Surfaces. *J. Tribol.* **2004**, *126*, 34–40. [[CrossRef](#)]
34. Zhang, Y.; Kovalev, A.; Hayashi, N.; Nishiura, K.; Meng, Y. Numerical Prediction of Surface Wear and Roughness Parameters during Running-In for Line Contacts Under Mixed Lubrication. *J. Tribol.* **2018**, *140*, 061501/1–061501/13. [[CrossRef](#)]
35. Kimura, Y.; Sugimura, J. Microgeometry of sliding surfaces and wear particles in lubricated contact. *Wear* **1984**, *100*, 33–45. [[CrossRef](#)]
36. Sugimura, J.; Kimura, Y. Characterization of topographical changes during lubricated wear. *Wear* **1984**, *98*, 101–116. [[CrossRef](#)]
37. Sugimura, J.; Kimura, Y.; Amino, K. Analysis of the Topographical Changes Due to Wear—Geometry of the Running-In Process. *J. Jpn. Soc. Lubr. Eng.* **1986**, *31*, 813–820.
38. Mukras, S.M.S. Computer Simulation/Prediction of Wear in Mechanical Components. *Adv. Tribol.* **2020**, *2020*, 1–15. [[CrossRef](#)]
39. Neale, M.J. *The Tribology Handbook*, 2nd ed.; Butterworth-Heinemann: Oxford, UK, 1995; ISBN 0750611987.

40. Bruce, R.W. *Handbook of Lubrication and Tribology: Volume II: Theory and Design*, 2nd ed.; CRC Press: Boca Raton, FL, USA, 2012; ISBN 9781420069099.
41. Hansen, J.; Björling, M.; Larsson, R. Mapping of the lubrication regimes in rough surface EHL contacts. *Tribol. Int.* **2019**, *131*, 637–651. [[CrossRef](#)]
42. Hansen, J.; Björling, M.; Larsson, R. Lubricant film formation in rough surface non-conformal conjunctions subjected to GPa pressures and high slide-to-roll ratios. *Sci. Rep.* **2020**, *10*, 22250/1–22250/16. [[CrossRef](#)]
43. Hansen, J.; Björling, M.; Larsson, R. A New Film Parameter for Rough Surface EHL Contacts with Anisotropic and Isotropic Structures. *Tribol. Lett.* **2021**, *69*, 37/1–37/17. [[CrossRef](#)]
44. Jackson, R.L.; Green, I. A Finite Element Study of Elasto-Plastic Hemispherical Contact against a Rigid Flat. *J. Tribol.* **2005**, *127*, 343–354. [[CrossRef](#)]
45. Jackson, R.L.; Green, I. A statistical model of elasto-plastic asperity contact between rough surfaces. *Tribol. Int.* **2006**, *39*, 906–914. [[CrossRef](#)]
46. Jackson, R.L.; Green, I. The Behavior of Thrust Washer Bearings Considering Mixed Lubrication and Asperity Contact. *Tribol. Trans.* **2006**, *49*, 233–247. [[CrossRef](#)]
47. Bush, A.W.; Gibson, R.D.; Keogh, G.P. The limit of elastic deformation in the contact of rough surfaces. *Mech. Res. Commun.* **1976**, *3*, 169–174. [[CrossRef](#)]
48. McCool, J.I. Relating Profile Instrument Measurements to the Functional Performance of Rough Surfaces. *J. Tribol.* **1987**, *109*, 264–270. [[CrossRef](#)]
49. Beheshti, A.; Khonsari, M.M. Asperity micro-contact models as applied to the deformation of rough line contact. *Tribol. Int.* **2012**, *52*, 61–74. [[CrossRef](#)]
50. Tomota, T.; Masuda, R.; Kondoh, Y.; Ohmori, T.; Yagi, K. Modeling Solid Contact between Rough Surfaces with Various Roughness Parameters. *Tribol. Trans.* **2021**, *64*, 178–192. [[CrossRef](#)]
51. Johnson, N.L. Systems of Frequency Curves Generated by Methods of Translation. *Biometrika* **1949**, *36*, 149–176. [[CrossRef](#)] [[PubMed](#)]
52. Elderton, W.P.; Johnson, N.L. *Systems of Frequency Curves*; Cambridge University Press: Cambridge, UK, 1969; ISBN 9780511569654.
53. Yu, N.; Polycarpou, A.A. Contact of Rough Surfaces with Asymmetric Distribution of Asperity Heights. *J. Tribol.* **2002**, *124*, 367–376. [[CrossRef](#)]
54. Habchi, W. *Finite Element Modeling of Elastohydrodynamic Lubrication Problems*; Wiley: Hoboken, NJ, USA, 2018; ISBN 9781119225126.
55. Marian, M.; Weschta, M.; Tremmel, S.; Wartzack, S. Simulation of Microtextured Surfaces in Starved EHL Contacts Using Commercial FE Software. *Mater. Perform. Charact.* **2017**, *6*, 165–181. [[CrossRef](#)]
56. Hughes, T.J.; Franca, L.P.; Hulbert, G.M. A new finite element formulation for computational fluid dynamics: VIII. The galerkin/least-squares method for advective-diffusive equations. *Comput. Methods Appl. Mech. Eng.* **1989**, *73*, 173–189. [[CrossRef](#)]
57. Zienkiewicz, O.C.; Taylor, R.L.; Nithiarasu, P. *The Finite Element Method for Fluid Dynamics*, 7th ed.; Butterworth-Heinemann: Oxford, UK, 2014; ISBN 9781856176354.
58. Dowson, D.; Higginson, G.R. *Elasto-Hydrodynamic Lubrication: SI-Edition*; Pergamon: Oxford, UK, 1977; ISBN 9780080213033.
59. Roelands, C.J.A. Correlational Aspects of the Viscosity-Temperature-Pressure Relationship of Lubricating Oils. Ph.D. Thesis, Technische Hogeschool Delft, Delft, The Netherlands, 1966.
60. Eyring, H. Viscosity, Plasticity, and Diffusion as Examples of Absolute Reaction Rates. *J. Chem. Phys.* **1936**, *4*, 283–291. [[CrossRef](#)]
61. Wriggers, P. *Computational Contact Mechanics*; Wiley: New York, NY, USA, 2002; ISBN 0471496804.
62. Bhushan, B. (Ed.) *Modern Tribology Handbook*; CRC Press: Boca Raton, FL, USA, 2001; ISBN 9780849384035.
63. Jeng, Y.-R.; Gao, C.-C. Changes of Surface Topography during Wear for Surfaces with Different Height Distributions. *Tribol. Trans.* **2000**, *43*, 749–757. [[CrossRef](#)]
64. Jeng, Y.-R.; Lin, Z.-W.; Shyu, S.-H. A Microscopic Wear Measurement Method for General Surfaces. *J. Tribol.* **2002**, *124*, 829–833. [[CrossRef](#)]
65. Jeng, Y.-R.; Lin, Z.-W.; Shyu, S.-H. Changes of Surface Topography during Running-In Process. *J. Tribol.* **2004**, *126*, 620–625. [[CrossRef](#)]
66. Hamrock, B.J.; Dowson, D. *Ball Bearing Lubrication: The Elastohydrodynamics of Elliptical Contacts*; Wiley: New York, NY, USA, 1981; ISBN 9780471035534.
67. *DIN 51819-1*; Prüfung von Schmierstoffen—Mechanisch-dynamische Prüfung auf dem Wälzlagerschmierstoff-Prüfgerät FE8—Teil 1: Allgemeine Arbeitsgrundlagen. Beuth: Berlin, Germany, 2016.
68. *DIN 51819-3*; Prüfung von Schmierstoffen—Mechanisch-dynamische Prüfung auf dem Wälzlagerschmierstoff-Prüfgerät FE8—Teil 3: Verfahren für Schmieröl-einzusetzende Prüflager: Axialzylinderrollenlager. Beuth: Berlin, Germany, 2016.